Reprogrammable optical phase array

Madeleine Mony,[1,*] Eric Bisaillon,[1] Ehab Shoukry,[1] Christopher Ostafew,[1] Etienne Grondin,[2] Vincent Aimez,[2] and David V. Plant[1]

[1]Electrical and Computer Engineering, McGill University, 3480 University Street, Montreal QC, H3A 2A7, Canada
[2]Electrical and Computer Engineering, Université de Sherbrooke, Sherbrooke QC, J1K 2R1, Canada

*Corresponding author: maddy@photonics.ece.mcgill.ca

Received 27 November 2006; accepted 5 January 2007;
posted 16 March 2007 (Doc. ID 77459); published 31 May 2007

A novel reprogrammable optical phase array (ROPA) device is presented as a reconfigurable electro-optic element. One specific application of the ROPA, a 1×6 electro-optic space switch, is fully described. Switching angles are within 2°, and switching is achieved through a complementary metal-oxide semiconductor (CMOS) controlled, diffraction based, optical phase array in a bulk $BaTiO_3$ crystal. The crystal is flip-chipped to the CMOS chip, creating a compact fully integrated device. The design, optical simulation, and fabrication of the device are described, and preliminary experimental results are presented. © 2007 Optical Society of America

OCIS codes: 230.2090, 050.5080.

1. Introduction

Diffractive optical elements (DOEs) perform many optical functions, but their optical behavior remains fixed after fabrication. We present a novel reprogrammable optical phase array (ROPA) that can behave as a reconfigurable DOE, suitable for such applications as beam focusing at different focal lengths, multiple spot generation, active beam distortion compensation, and operating as an adaptive multiwavelength switch. The ROPA design consists of applying multiple electric fields of different magnitudes across an electro-optic (EO) material. The configuration of the electric fields can be shaped to create different optical structures. In this paper, we explore one particular application of the ROPA as a 1×6 space switch suitable for use within an agile all-photonic network.

Agile all-photonic networks require fast (μs) spatial switching at the core to allow for dynamic provisioning and optical packet switching [1]. EO switches fulfill these requirements, but both waveguide and bulk EO switches have significant drawbacks: in the waveguide structure the coupling losses can be high, and in the bulk structure the required voltages approach 1 kV [2]. The ROPA switch uses voltage levels below 300 V and in practice does not suffer from high coupling losses [3]. Another approach to optical space switching is to use optical phase arrays either based on a liquid-crystal design, and therefore with switching speeds of the order of milliseconds [4,5], or optical phase arrays with a small number of electrodes, which results in very high optical losses [6,7]. The ROPA design exploits the fast switching speeds of EO crystals, while having a large number of electrodes to maximize the overall diffraction efficiency.

In Section 2 we present the general ROPA design, and a simplified ROPA design used for space switching. In Section 3 we explore the choice of EO crystal and its effect on the design, and in Section 4 we present the optical simulations of the device performance. Finally, in Section 5 we discuss the processing steps for the EO crystal, and in Section 6 we present the preliminary experimental results.

2. Reprogrammable Optical Phase Array Design

The ROPA switch is a reflective, diffractive optical element and is shown in Fig. 1. Electrodes are deposited onto an EO crystal to allow the electrical induction of arbitrary index changes within the crystal. The crystal is in turn flip-chipped to a CMOS chip. The incident light travels through the electro-optic crystal and reflects off of the metallic electrodes in

0003-6935/07/183724-06$15.00/0

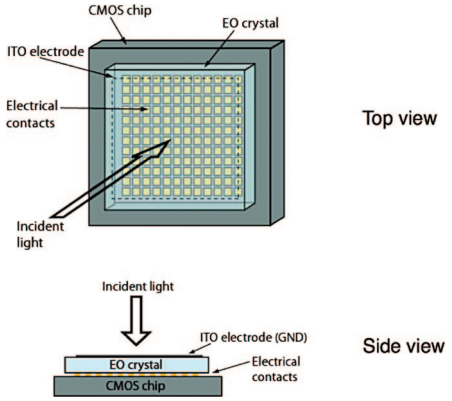

Fig. 1. (Color online) General ROPA concept.

between the EO material and the CMOS chip. Voltages are applied to the metal electrodes by the CMOS chip, and a pattern of different refractive indices is induced in the electro-optic material. The profile of the device can be reconfigured by changing these voltages.

The integrated ROPA device is small (<1 cm^2) and has a fast response time (μs), which is limited by the speed of the CMOS chip. The response time of the EO crystal itself is of the order of nanoseconds. One of the great strengths of the ROPA device is its ability to handle different wavelengths. This is because the magnitude of the phase change experienced by the incident light is controlled through the voltages applied to the electrodes. The main drawback of the device is that it is less efficient than a conventional DOE due to the difficulty in generating arbitrary electric fields within the bulk of the EO material.

A simplified design of the ROPA is shown in Fig. 2. This design reduces the number of electrodes, which in turn reduces the number of independent voltages required to control the device. This allows for a simpler CMOS design. However, since the voltages now vary across only one dimension of the EO material, the incoming beam can only be steered in one dimension. By varying the number of electrodes per grating period, the angle of the first-order diffraction changes and the beam is redirected to a different output port. We have fabricated this version of the ROPA device, to be used as a hitless 1×6 space switch.

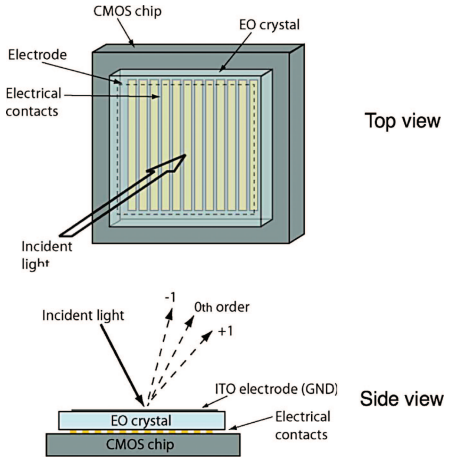

Fig. 2. (Color online) Simplified ROPA, used as a 1×6 space switch.

The EO crystal is placed between a transparent grounded indium tin oxide (ITO) electrode and an array of 64 reflective metal electrodes. The electrodes are 20 μm wide with a 5 μm gap between them, which gives a fill factor of 80%. The 5 μm gap is necessary to prevent electrical breakdown between the electrodes. Through the voltages that are applied to the metal electrodes by the CMOS chip, a blazed diffraction grating is induced in the electro-optic material. The grating diffracts the reflected light into the $+1$ or -1 diffractive orders. The angular deflection is dependent on the chosen periodicity of the grating, which is defined by the voltages.

The CMOS chip is made using a high-voltage CMOS process in which low-voltage and high-voltage (HV) circuits can be implemented [8]. The chip design consists of an array of 64 digital-to-analog controllers (DACs) that independently provide voltages up to 300 V to each of the 64 electrodes across the electro-optic crystal. This maximum voltage provided by the chip greatly influences the choice of electro-optic crystal, as discussed in the next section.

3. Electro-Optic Crystal

The electric field is applied across the thickness of the crystal, thus inducing an index change in the EO crystal. The change in index when the maximum voltage is applied (300 V) must be sufficient to introduce a 2π phase shift to the incident light. The magnitude of the index change is determined by the tensor of electro-optic coefficients for the crystal, which is multiplied by the applied electric field.

In commonly used EO crystals, lithium niobate ($LiNbO_3$), for example, the strongest EO coefficient is the r_{33} coefficient. However, this coefficient is not appropriate for the ROPA design. Since a large component of the light propagates collinearly with the electric field direction, the ideal index change is perpendicular to the applied electric field. $BaTiO_3$ crystals, on the other hand, have a very strong r_{15} coefficient (1700 pm/V) [9]. The EO tensor for $BaTiO_3$ is shown below, with units of pm/V:

$$r_{ij} = \begin{bmatrix} 0 & 0 & 12 \\ 0 & 0 & 12 \\ 0 & 0 & 112 \\ 0 & 1700 & 0 \\ 1700 & 0 & 0 \\ 0 & 0 & 0 \end{bmatrix}. \quad (1)$$

The crystal orientation with respect to the incident light is shown in Fig. 3. For a $BaTiO_3$ crystal, when the electric field is applied along the x axis, the resultant index ellipsoid is

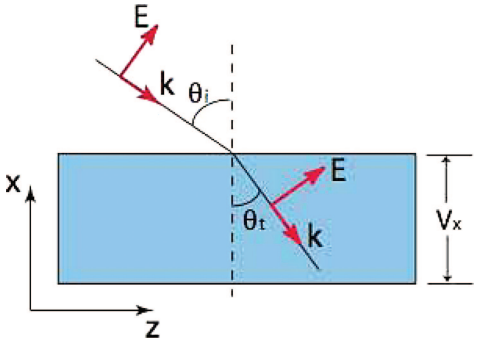

Fig. 3. (Color online) Incidence angle of light onto crystal.

$$\frac{x^2}{n_o^2}+\frac{y^2}{n_o^2}+\frac{z^2}{n_e^2}+2r_{51}E_x xz=1, \tag{2}$$

where n_o and n_e are the material ordinary and extraordinary refractive indices, respectively. Since there is no index change along the y axis for a nonzero electric field applied along the x axis, we can consider only the xz plane. If we graphically plot the index ellipsoid for the cases where $E_x = 0$ and $E_x \gg 1$, we get the ellipse shown in Fig. 4.

As can be seen in Fig. 2, to get the largest index change when applying an electric field along the x axis, the incident light must propagate within the crystal along the $x = z$ direction (i.e., at 45° from both the x and z axes). Due to the high index of refraction of the crystal ($n_o = 2.31$, $n_e = 2.28$ at 1300 nm), it is not possible to have incident light refract and enter the crystal with an angle higher than the critical angle ($\theta_c = 25°$). However, when the light is incident onto the crystal near the Brewster angle ($\theta_i = \theta_B = 65°$), the light within the crystal propagates at $\theta_t = 22°$.

Let θ_t define the direction of the propagation of the light within the crystal, and let θ define the direction of propagation of the electric field within the crystal. When there is no electric field applied to the crystal ($E_x = 0$), the index of refraction sampled by the incoming light is

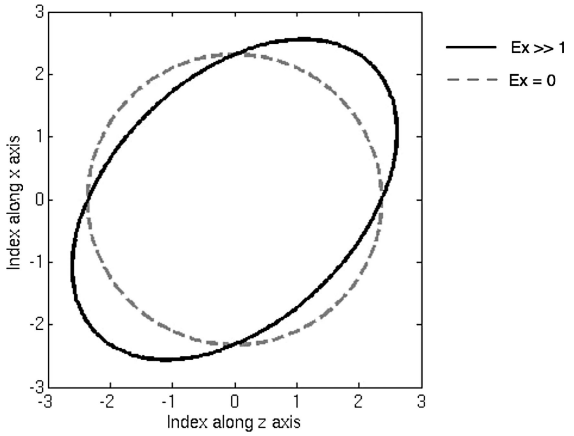

Fig. 4. Index ellipsoid of $BaTiO_3$ when voltage is applied along the x axis.

$$n=\frac{\left[\dfrac{1}{(\tan\theta * n_o)^2}+\dfrac{1}{n_e^2}\right]^{-1/2}}{\sin\theta}. \tag{3}$$

When there is an electric field applied to the crystal along its x axis, the index of refraction becomes

$$n_{E_x}=\frac{\left[\dfrac{1}{(\tan\theta * n_o)^2}+\dfrac{1}{n_e^2}+\dfrac{2r_{51}E_x}{\tan\theta}\right]^{-1/2}}{\sin\theta}. \tag{4}$$

The change in refractive index seen by the light can be determined by subtracting Eq. (3) from Eq. (4), i.e., $\Delta n = n_{E_x} - n$.

One drawback of choosing $BaTiO_3$ as the EO crystal for the switch is that it must be kept within 13 °C and 125 °C. $BaTiO_3$ will undergo a phase change to become orthorhombic when the temperature is lowered below 13 °C, or to become cubic when it is raised above 125 °C. When it returns to its tetragonal state at room temperature, it has lost molecular polarization and is unusable without repoling.

4. Simulations

In order to simulate the optical performance of the ROPA we exploit the quasi-periodic nature of the device by using the rigorous coupled-wave analysis (RCWA) technique [10]. In addition to the conventional implementation of RCWA, we have developed a novel iterative modeling algorithm for uniaxial periodic EO materials. This algorithm, described in the following sections, involves calculating and segmenting the index profile of the crystal, determining the diffraction efficiency of the grating, and then using a simulated annealing technique to iteratively tune the electrode voltages to improve the diffraction efficiency.

A. Determining Refractive Index Profile

Electrode voltages are applied as boundary conditions to the EO crystal, and the electric field distribution is subsequently computed using a finite-difference modeling method. Once the electric field distribution has been found, the resulting indices of refraction are calculated at each point in the crystal using the EO tensor, as is the index of refraction for a given optical path through the material. Due to the anisotropic nature of the crystal, the index sampled by light once reflected from the bottom electrodes will be different from that before reflection. In order to circumvent this added difficulty in the subsequent simulations, the postreflection path through the structure is unfolded in the model yielding a pure transmission structure, through which light propagation is unidirectional. The unfolded index profile for a single grating period consisting of four electrodes (a period of 100 μm), with voltages 0, 100, 200, and 300 V, is shown in Fig. 5.

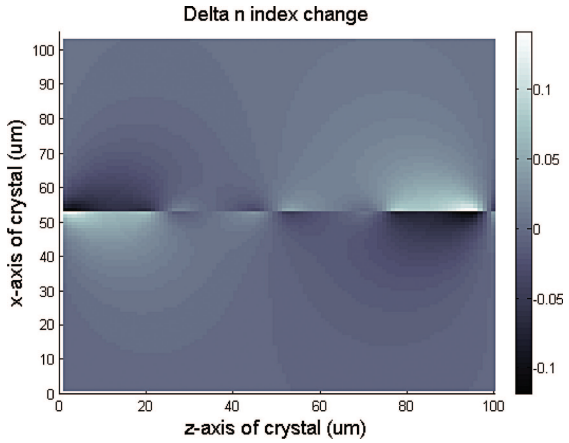

Fig. 5. (Color online) Index change (Δn) of center of unfolded $BaTiO_3$.

B. Segmentation of Index Profile

The computed index profile for the unfolded structure is transferred into a two-dimensional RCWA algorithm. This index profile is segmented in both spatial directions into uniform index segments. The number of segments depends on the index profile and care must be taken to ensure that for a given number of segments die computation is convergent. The transmission efficiencies of the structure are obtained in the RCWA.

C. Optimization of Diffraction Efficiencies

In order to optimize the voltages applied to the structure, the entire model is executed in a simulated annealing optimization process. This optimization uses the efficiency in the desired order(s) as the merit function with the voltage variation linked to the simulated annealing temperature parameter. The simulated annealing optimization can be applied to all of the electrodes simultaneously or to one electrode at a time, and this can be done repeatedly for a further refinement of the design.

Figure 6 shows the simulated diffraction efficiencies of the ROPA device, working at 1310 nm, which range from 37% to 63%. The x axis indicates the number of electrodes in one period of the grating. As the number of electrodes increases, the ability to tailor the profile of the grating increases, leading to greater diffraction efficiencies. However, an increasing period leads to a reduction in the deflection angle. When using three to eight electrodes per period, the deflection angles range from $\pm 0.38°$ to $\pm 1.0°$ about the zero-order reflection. For a crystal thickness of 500 μm, the voltage needed for a 2π phase shift is 295 V. When working at 1550 nm, as shown in Fig. 7, the diffraction efficiencies range from 39% to 62%, but the required maximum voltage is 355 V.

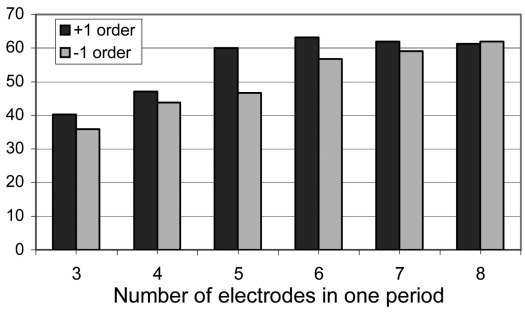

Fig. 6. Diffraction efficiencies for device used at 1310 nm.

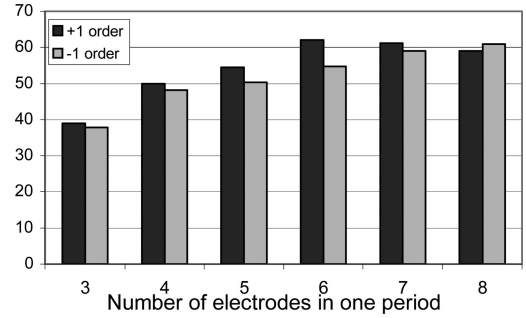

Fig. 7. Diffraction efficiencies for device used at 1550 nm.

D. Effect of Finite Grating

The RCWA simulations in the previous subsection assume an infinite grating. The finite number of periods in the ROPA device will result in a larger angular width of the diffracted-order angles. In our case, the number of periods is dependent on the periodicity of the grating, i.e., the number of electrodes used per period. Additionally, the RCWA simulations assume plane-wave incidence, whereas the incident beam for our device will be a Gaussian beam with a waist of 640 μm. Taking both of these factors into account yields the diffraction angle spread shown in Table 1, where θ is the angle of diffraction given by the scalar grating equation.

In order to minimize cross talk, a 1×6 switch is realized by tuning the electrode voltages for either the $+1$ or -1 orders, for a grating consisting of three, five, or eight electrodes per period. The corresponding entries in the table are shown in bold. The zeroth diffraction order is not used for the switch, as that output port would suffer from high cross talk. This is especially true when switching light to the first, order using only three electrodes per period, as that is the configuration that suffers from the lowest diffraction efficiency.

Table 1. Diffraction Angle Spread for Finite Periods and Incident Gaussian Beam

Electrodes per Period	Period of Grating	Periods	θ	Diffraction Angle Spread
8	**200 μm**	**8**	**0.59°**	**0.48° to 0.70°**
7	175 μm	9	0.67°	0.56° to 0.78°
6	150 μm	10	0.78°	0.67° to 0.90°
5	**125 μm**	**12**	**0.94°**	**0.83° to 1.06°**
4	100 μm	16	1.18°	1.07° to 1.29°
3	**75 μm**	**21**	**1.58°**	**1.47° to 1.70°**

5. Crystal Processing

The processing of the crystal involves cutting, polishing, poling, and then depositing the electrodes. The cutting and the polishing must be performed before poling because the compressive stress experienced during polishing can induce reorientation of the 90° domains in the crystal [11]. The crystal is cut to 5 mm × 5 mm × 0.5 mm. The poling is performed by applying an electric field of 1.5 kV/mm, while slowly decreasing the temperature from 135 °C to room temperature.

The electrodes need to adhere to the crystal, to be compatible with the flip-chip process, and to be highly reflective at 1310 nm. Aluminum (Al) is highly reflective at telecom wavelengths (97% at 1310 nm), but unfortunately does not adhere well to the EO crystals. Therefore, a thin layer of titanium (Ti) is necessary between the crystal and the Al electrode. This layer reduces the reflectivity of the electrodes, so it is chosen to be as thin as possible, i.e., 50 angstroms. In order to be compatible with flip-chipping, a thick layer of gold (>3000 angstroms) needs to be deposited as the top layer of the electrodes. A layer of Ti is necessary to act as a barrier layer between the Al and the Au layers. The final stack-up of the electrodes is Ti/Al/Ti/Au with thicknesses of 50/500/500/6000 angstroms, respectively. The simulated reflectivity of the electrodes is 90% at 1310 nm, and it is 89% at 1550 nm.

6. Preliminary Experimental Results

The experimental results to date involves the complete testing and characterization of the CMOS chip, the deposition of electrodes onto the EO crystal, flip-chipping the EO crystal onto test chips, and some preliminary optical testing of the device.

A. High-Voltage Complementary Metal-Oxide Semiconductor Chip

The high-voltage chip was fabricated in Dalsa Semiconductor's 0.8 μm complementary/diffused metal-oxide semiconductor (CMOS/DMOS) HV process technology. The design consists of an array of 64 DAC converters capable of providing up to 300 [12]. Once the EO crystal is flip-chipped to the high-voltage chip, each DAC independently controls the voltage for one electrode on the crystal. The location of the flip-chip pads and of one of the DACs in the array are highlighted in Fig. 8 below. In order to not affect the optical performance of the crystal flip-chipped to the chip, a thermo-electric cooler is used to actively cool the chip to room temperature.

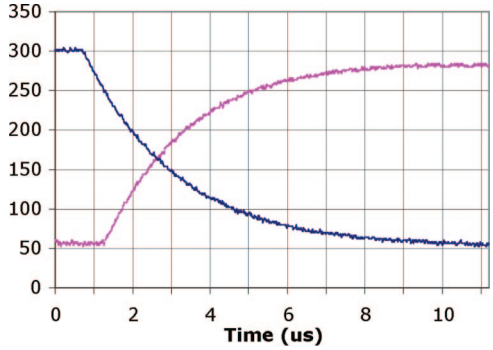

Fig. 9. (Color online) Switching speeds when DAC is providing the maximum output swing.

The design of the DACs is based on a current-steering, thermometer coded architecture. The DACs are 6-bit, which gives a voltage resolution of 4.76 V for output voltages ranging from 0 V to 300 V. The current to HV conversion is done using a high-compliance current mirror adapted to the HV technology.

An important parameter for the DAC performance is the switch time. The switch time is measured for the case when the DAC is providing the maximum output voltage swing and is shown in Fig. 9. The capacitance of each electrode is 3.9 pF. The experimentally measured rise time (10% to 90%) is less than 5.4 μs, and the fall time is less than 16.2 μs.

B. Optical Testing

The EO crystals were processed as described in Section 5. The measured reflectivity of the electrodes at 1310 nm is 67%, and at 1550 nm it is 64% with an error of 5% on the measurement. The experimentally measured reflectivity is lower than the simulated re-

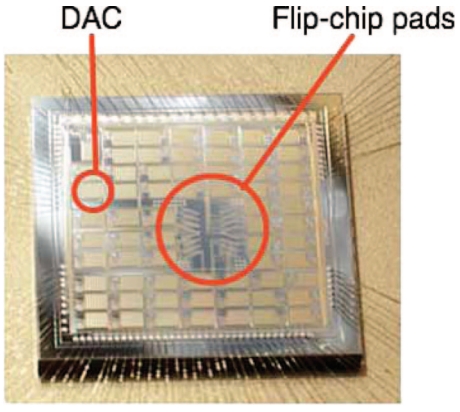

Fig. 8. (Color online) Packaged high-voltage chip.

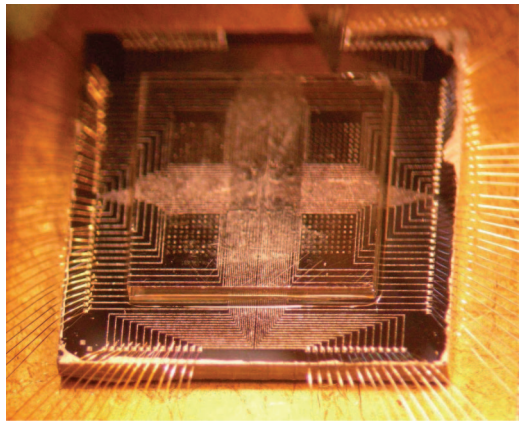

Fig. 10. (Color online) EO crystal flip-chipped onto test chip.

flectivity, discussed in Section 5, due to roughness scattering.

The crystal was then flip-chipped onto a test chip, as shown in Fig. 10 below. The bump bonds are 20 μm × 20 μm and are 2.5 μm thick.

The light incident onto the EO crystal is TM polarized with respect to the electrodes and has an extinction ratio of >35 dB. The measured insertion loss of the zeroth-order mode through the bulk crystal is 1.32 dB. A switching extinction ratio of 5 dB has currently been obtained for a periodicity of five electrodes per period.

7. Conclusion

The ROPA switch presented is a fast, low-voltage (<300 V), 1 × 6 optical switch, suitable for use within an agile all-photonic network. The output beam is directed to the correct output port of the switch by changing the number of electrodes used per grating period. It takes advantage of the full voltage range offered by the high-voltage CMOS chip, and it is a compact, heterogeneously integrated device. By using our novel iterative simulation technique, the voltages have been optimized to provide simulated diffraction efficiencies in the range of 36% to 64%, with up to a ±1.58° switching angle.

References

1. L. Mason, A. Vinokurov, N. Zhao, and D. Plant, "Topological design and dimensioning of agile all-photonic networks," Comput. Netw. **50,** 268–287 (2006).
2. Y. Zuo, B. Bahamin, E. J. Tremblay, C. Pulikkaseril, E. Shoukry, M. Mony, P. Langlois, V. Aimez, and D. V. Plant, "1 × 2 and 1 × 4 electrooptic switches," Photon. Technol. Lett. **17,** 2080–2082 (2005).
3. M. Mony, E. Bisaillon, K. W. Goossen, E. Shoukry, and D. V. Plant, "Reprogrammable optical phase array (ROPA) for use in an agile all-photonic network," *OSA Information Photonics Topical Meeting* (Optical Society of America, 2005), paper IWB3.
4. P. F. McManamon, T. A. Dorschner, D. L. Corkum, L. J. Friedman, D. S. Hobbs, M. Holz, S. Liberman, H. Q. Nguyen, D. P. Resler, R. C. Sharp, and E. A. Watson, "Optical phased array technology," Proc. IEEE **84,** 268–298 (1996).
5. S. Serati and J. Stockley, "Advanced liquid crystal on silicon optical phased arrays," IEEE Aerospace Conf. Proc. **3,** 1395–1402 (2002).
6. R. A. Meyer, "Optical beam steering using a multichannel lithium tantalate crystal," Appl. Opt. **11,** 613–616 (1972).
7. J. A. Thomas and Y. Fainman, "Programmable diffractive optical element using a multichannel lanthanum-modified lead zirconate titanate phase modulator," Opt. Lett. **20,** 1510–1512 (1995).
8. M. J. M. Pelgrom, "A 10-b 50-MHz CMOS D/A converter with 75-Ω buffer," IEEE J. Solid-State Circuits **25,** 1347–1352 (1990).
9. MTI Corporation, "$BaTiO_3$ specifications," http://www.mticrystal.com.
10. M. G. Moharam and T. K. Gaylord, "Rigorous coupled-wave analysis of planar-grating diffraction," J. Opt. Soc. Am. **71,** 811–818 (1981).
11. N. J. Poole, "Effects of aging and compressive stress on the properties of $BaTiO_3$ ceramics," J. Phys. D **8,** 1140–1148 (1975).
12. E. Shoukry, M. Mony, and D. V. Plant, "Design of a fully integrated array of high-voltage digital-to-analog converters," in *IEEE International Symposium on Circuits and Systems* (IEEE, 2005), pp. 372–375.